Quasi-near field terahertz generation and detection.

Reshmi Chakkittakandy[1], Jos. A. W. M. Corver[2] and Paul C. M. Planken[1]

[1]*Department of Imaging Science and Technology, Faculty of Applied Sciences, Delft University of Technology, Lorentzweg 1, 2628 CJ Delft, The Netherlands*

[2]*IMA Edwards Freeze Drying Solutions, Steenstraat 7, 5107 NE Dongen, The Netherlands.*

r.chakkittakandy@tudelft.nl

Abstract: We describe a simple terahertz (THz) time domain spectrometer with a bandwidth extending up to 7.5 THz. We show that by keeping the generation and detection crystals close to each other a high signal-to-noise ratio (SNR) can be achieved without using lock-in detection and dry nitrogen flushing. The observed spectra show very good agreement with the spectra calculated based on a simple model which includes phase matching and absorption in the generation and detection crystals. Using this set-up we have measured the absorption lines in D-tartaric acid from 0.5 THz up to 7 THz. We show that the high frequency region $>$ 3 THz is the better choice to measure small changes in the water content of a hygroscopic sample compared to the low frequency region.

OCIS codes: (040.2235) Far infrared or terahertz; (300.6495) Spectrosopy, THz; (320.7160) Ultrafast technology.

References and links

1. M. van Exter, C. Fattinger, and D. Grischkowsky, "Terahertz time-domain spectroscopy of water vapor," Opt. Lett. **14**, 1128–1131 (1989).
2. Y. R. Shen, "Far-infrared generation by optical mixing," Prog. Quantum Electron. **4**, 207–232 (1976).
3. L. Xu, X.-C. Zhang, and D. H. Auston, "Terahertz beam generation by femtosecond optical pulses in electro-optic materials," Appl. Phys. Lett. **61**, 1784–1786 (1992).
4. C. Kubler, R. Huber, and A. Leitenstorfer, "Ultrabroadband terahertz pulses:generation and field-resolved detection," Semicond. Sci. Technol. **20**, S128–S133 (2005).
5. A. Leitenstorfer, S. Hunsche, J. Shah, M. C. Nuss, and W. H. Knox, "Detectors and sources for ultrabroadband electro-optic sampling: Experiment and theory," Appl. Phys. Lett. **74**, 1516–1518 (1999).
6. Q. Wu and X.-C. Zhang, "Free-space electro-optic sampling of terahertz beams," Appl. Phys. Lett. **67**, 3523–3525 (1995).
7. A. Nahata, A. S. Weling, and T. F. Heinz, "A wideband coherent terahertz spectroscopy system using optical rectification and electro-optic sampling," Appl. Phys. Lett. **69**, 2321–2323 (1996).
8. D. Mittleman, R. Jacobsen, and M. Nuss, "T-ray imaging," IEEE J. Sel. Top. Quantum Electron. **2**, 679–692 (1996).
9. D. M. Mittleman, R. H. Jacobsen, R. Neelamani, R. G. Baraniuk, and M. C. Nuss, "Gas sensing using terahertz time-domain spectroscopy," Appl. Phys. B **67**, 379–390 (1998).
10. J. M. Chamberlain, "Where Optics Meets Electronics: Recent Progress in Decreasing the Terahertz Gap," Phil. Trans. R. Soc. Lond. A **362**, 199–213 (2004).
11. G. C. . Cho, P. Y. Han, X. C. Zhang, and H. J. Bakker, "Optical phonon dynamics of GaAs studied with time-resolved terahertz spectroscopy," Opt. Lett. **25**, 1609–1611 (2000).
12. D. Grischkowsky, S. Keiding, M. van Exter, and C. Fattinger, "Far-infrared time-domain spectroscopy with terahertz beams of dielectrics and semiconductors," J. Opt. Soc. Am. B **7**, 2006–2015 (1990).

#98668 - $15.00 USD Received 11 Jul 2008; revised 4 Aug 2008; accepted 5 Aug 2008; published 7 Aug 2008

13. M. van Exter, C. Fattinger, and D. Grischkowsky, "High-brightness terahertz beams characterized with an ultrafast detector," Appl. Phys. Lett. **55**, 337–339 (1989).
14. N. C. J. van der Valk and P. C. M. Planken, "Electro-optic detection of subwavelength terahertz spot sizes in the near field of a metal tip." Appl. Phys. Lett. **81**, 1558–1560 (2002).
15. M. A. Seo, A. J. L. Adam, J. H. Kang, J. W. Lee, S. C. Jeoung, Q. H. Park, P. C. M. Planken, and D. S. Kim, "Fourier-transform terahertz near-field imaging of one-dimensional slit arrays: mapping of electric-field-, magnetic-field-, and Poynting vectors," Opt. Express **15**, 11781–11789 (2007).
16. A. J. L. Adam, J. M. Brok, S. M. A., K. J. Ahn, D. S. Kim, J. H. Kang, Q. H. Park, M. Nagel, and P. C. M. Planken, "Advanced terahertz electric near field measurements at subwavelength diameter metallic apertures," Opt. Express **16**, 7407–7417 (2008).
17. P. U. Jepsen, C. Winnewisser, M. Schall, V. Schyja, S. R. Keiding, and H. Helm, "Detection of THz pulses by phase retardation in lithium tantalate," Phys. Rev. E **53**, R3052–R3054 (1996).
18. G. Zhao, R. N. Schouten, N. van der Valk, and W. T. Wenckebach, "Design and performance of a THz emission and detection setup based on a semi-insulating GaAs emitter," Rev. Sci. Instrum. **73**, 1715–1719 (2002).
19. N. C. J. van der Valk, P. C. M. Planken, A. N. Buijserd, and H. J. Bakker, "Influence of pump wavelength and crystal length on the phase matching of optical rectification," J. Opt. Soc. Am. B **22**, 1714–1718 (2005).
20. H. J. Bakker, G. C. Cho, H. Kurz, Q. Wu, and X.-C. Zhang, "Distortion of terahertz pulses in electro-optic sampling," J. Opt. Soc. Am. B **15**, 1795–1801 (1998).
21. J. Faure, J. Van Tilborg, R. A. Kaindl, and W. P. Leemans, "Modelling Laser-Based Table-Top THz Sources: Optical Rectification, Propagation and Electro-Optic Sampling," Opt. Quantum Electron. **36**, 681–697 (2004).
22. B. M. Fischer, M. Hoffmann, H. Helm, G. Modjesch, and P. U. Jepsen, "Chemical recognition in terahertz time-domain spectroscopy and imaging," Semicond. Sci. Technol **20**, 246–253 (2005).
23. B. M. Fischer, H. Helm, and P. U. Jepsen, "Chemical recognition with broad band THz spectroscopy," Proc. IEEE **95**, 1592–1604 (2007).

1. Introduction

Terahertz Time-Domain Spectroscopy (THz-TDS) is a technique in which femtosecond laser pulses are used to generate and coherently detect broadband THz electric-field transients [1]. One mechanism often used to generate these THz pulses is optical rectification [2]. In this method, an ultra short optical pulse is focused onto a non-linear crystal such as ZnTe or GaP, where it generates a polarization in the crystal that follows the envelope of the pulse [3]. Using this technique, ultra broadband THz pulses with a spectrum extending from 100 GHz to 60 THz have been generated [4, 5]. To detect the time-dependent electric field of these pulses, electro-optic sampling can be used [6]. In electro-optic sampling, a THz pulse co-propagates with the probe pulse inside an electro-optic crystal. In the crystal, the instantaneous THz electric-field elliptically polarizes the probe pulse. This ellipticity can be measured using a standard differential detection setup and by measuring the amount of ellipticity as a function of the optical delay between the THz electric field and the probe laser pulse, the THz electric-field as a function of time can be measured in a stroboscopic manner. For efficient generation and detection of THz radiation using optical rectification and electro-optic sampling respectively, it is important that the phase velocity of the THz radiation equals the group velocity of the pump/probe pulse [7]. A phase mismatch can, for example, reduce the bandwidth of the detected THz electric fields. For this reason generally thin crystals, down to $\leq 10\mu$m thickness, have to be used to detect the extremely high frequencies up to 60 THz [4, 5].

THz-TDS is a very important technique that can be used for imaging [8], and for the observation of rotational transitions in molecular gases and lattice modes in molecular crystals [9, 10, 11]. A very attractive property of THz-TDS is that it gives both amplitude and phase information about the samples being investigated [12]. However, most THz-TDS setups suffer from a number of problems. First, a typical THz-TDS setup requires parabolic mirrors to collimate, steer and focus the THz radiation onto the detection crystal [13]. Unfortunately, parabolic mirrors are notoriously difficult to align, especially considering that THz radiation is invisible. Second, the long THz beam path through air in a typical THz-TDS setup requires that the beam path be flushed with dry N_2 gas to reduce the absorption of the THz radiation

#98668 - $15.00 USD Received 11 Jul 2008; revised 4 Aug 2008; accepted 5 Aug 2008; published 7 Aug 2008

by water vapor molecules in the atmosphere. Third, since optical rectification is usually not very efficient to convert laser light into THz light, losses in the THz beam by diffraction and by absorption at reflecting surfaces in the THz beam path, lead to further reductions in the THz power. Fourth, to improve the Signal-to-Noise Ratio (SNR), the pump beam intensity is typically modulated in conjunction with lock-in-detection. However, modulation techniques often cause other problems, such as pulse lengthening when the laser pulses are sent through an acousto-optic modulator, or they cause vibrations when a mechanical chopper is used.

Here, we describe a method to generate and detect THz radiation using electro-optic crystals, in which the generation and detection crystals are placed close to each other and the THz pulses are generated and detected with, initially, counter-propagating pump and probe beams. Our set-up does not require parabolic mirrors to steer the THz beam, is intrinsically easy to align and does not suffer from the problems associated with the absorption of THz radiation by the water vapor molecules in the atmosphere. We demonstrate that such a quasi-near field setup gives us relatively strong signals and allows us to achieve a high SNR without using lock-in detection and without the need to flush the setup with dry nitrogen gas. We find that even with 500 μm thick generation and detection crystals of GaP, our setup allows us to achieve a THz generation/detection bandwidth of up to 7.5 THz. Our experimental results are in very good agreement with a simple theoretical model that includes phase-matching in both the generation and the detection crystal. Our results also imply that recent THz microscopy experiments [14, 15, 16], in which the probe pulse and the incident Thz pulse are initially counter propagating, can, in principle, detect near-field components with frequencies up to 7.5 THz. Our setup can easily be used for spectroscopic purposes by placing a sample between the generation and detection crystals. As an example, we show the measured absorption spectrum of D-tartaric acid for frequencies up to 7 THz. In addition, we show how our setup can be used to measure small changes in the water content of a hygroscopic sample, since this gives rise to pronounced absorption changes, especially at frequencies higher than $\approx$ 3 THz.

2. Experiments

Figure 1 shows our experimental setup. THz radiation is generated by optical rectification of 50 fs, 800 nm pulses from a Ti:sapphire oscillator (Scientific XL, Femtolasers) having a repetition rate of 11 MHz and an average power of 960 mW. The beam from the oscillator is split into two equal parts by a 50/50 beam splitter. One part (pump) is used to generate THz pulses and the other part (probe), is used to detect it. The pump beam is sent to an in-plane retroreflector mounted on a loudspeaker oscillating at 50 Hz, and is then focused onto a GaP generation crystal. The generation crystal has an Anti-Reflection (AR) coating on the surface through which the beam enters the crystal, to reduce reflection losses. It has a High Reflectivity (HR) coating on the opposite surface to prevent the pump beam from reaching the detection crystal and the differential detector. THz pulses, generated in the crystal, propagate a short distance of less than 1 mm through air, before entering a (110) oriented GaP detection crystal. From the back of the detection crystal, a synchronized probe pulse is focused onto the front surface, where the THz beam enters the crystal. The THz electric-field elliptically polarizes the probe beam with an amount equal to the instantaneous THz electric field value [17]. A HR coating on the front surface reflects the probe beam to a differential detector setup consisting of a quarter-wave plate, a Wollaston prism and a differential detector. This setup measures the ellipticity, and thus the instantaneous THz electric value. Since the optical delay between the pump pulse (and thus the THz pulse) and the probe pulse oscillates at 50 Hz, a full 25 ps long THz electric field time-trace is obtained every 20 ms [18]. We have used GaP crystals of 100 μm, 300 μm, or 500 μm thickness, both for the generation and the detection of THz radiation.

In order to perform spectroscopy of materials, samples can be inserted between the genera-

#98668 - $15.00 USD Received 11 Jul 2008; revised 4 Aug 2008; accepted 5 Aug 2008; published 7 Aug 2008

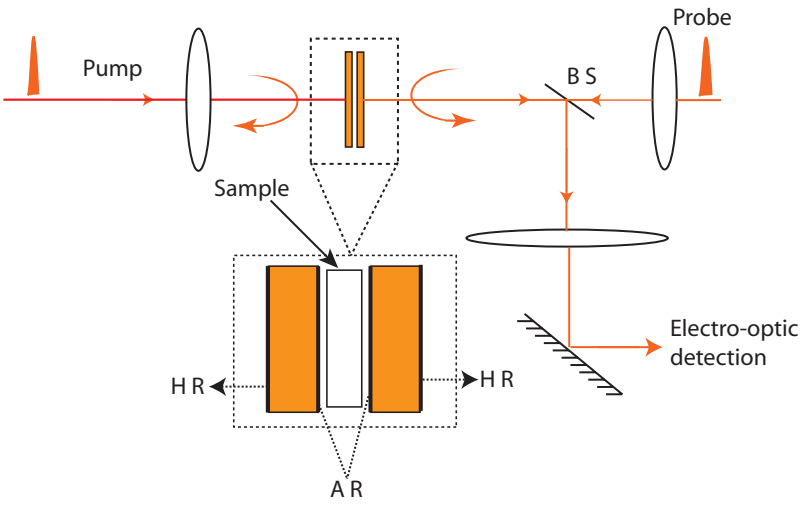

Fig. 1. Experimental set-up to generate and detect THz radiation in the quasi-near field. Both the generation and detection crystals have High Reflectivity (HR) coating on one surface and Anti Reflection (AR) coating on the other surface. The detection crystal is placed very close to the generation crystal with the HR surfaces facing each other. The probe beam is reflected back from the HR surface of the detection crystal and a beam splitter (BS) sends the pulse to a conventional electro-optic detection set-up.

tion and detection crystals. To prevent damage to the coating of the crystal, their HR surfaces are covered with a mylar foil of thickness 0.9 μm. The foil is completely transparent to the THz radiation.

3. Results and discussions

Figure 2(a)-(c) shows the temporal waveforms of the THz pulses detected with a GaP crystal of thickness 300 μm, and generated in GaP crystals of thicknesses 100 μm, 300 μm and 500 μm respectively. Figure 2(d)-(f) shows their corresponding amplitude spectra. In Fig. 3 we plot similar temporal wave forms and spectra to those shown in Fig. 2 except, in this case, the THz pulses are detected in a 100 μm thick crystal. In all these cases, the detected THz electric-field consists of a nearly single cycle initial pulse, followed by a rapidly oscillating decaying tail. As we will discuss below, this rapidly oscillating tail is due to phase matching in the generation crystal, where the phase velocity of the THz radiation is different from the group velocity of the pump pulse. The pulse ”echoes” appearing after the main pulse are from the reflection of the THz pulse in the generation and detection crystals. These reflections in the time domain will cause periodic oscillations in the frequency domain, thus complicating the analysis of any spectroscopic measurement. While calculating the spectra we have removed all reflections by taking only the data visible between the two doted lines in Fig. 2(a-c) and Fig. 3(a-c), and then zero-padded the data out to 40 ps before performing an FFT to calculate the spectra.

A comparison of Fig.’s 2 and 3 shows that GaP crystals of 300 μm thickness for both the generation and detection give a similar broad and flat spectrum up-to 7.5 THz, compared to the spectra obtained using generation and detection crystals of 100 μm thickness. The main

#98668 - $15.00 USD Received 11 Jul 2008; revised 4 Aug 2008; accepted 5 Aug 2008; published 7 Aug 2008

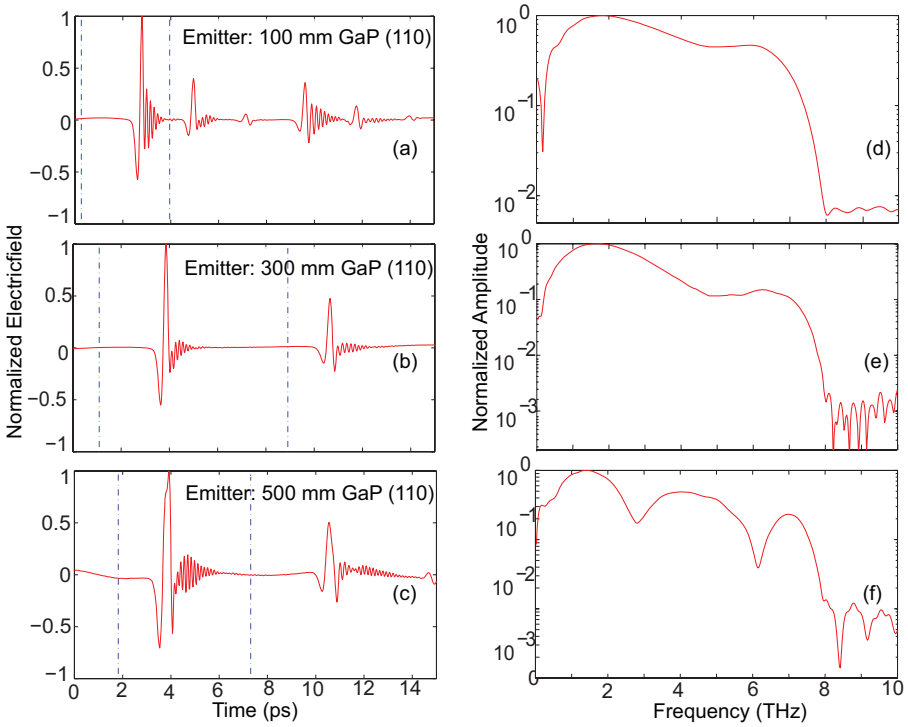

Fig. 2. (a)-(c) Measured temporal wave forms of THz pulses generated by a GaP (110) crystal and detected very close to the generation crystal with a 300 μm thick GaP (110) crystal (a)-(c) and their corresponding spectra (d)-(f). The figures are normalized to their maximum.

.

difference being that the 300 μm crystals have a somewhat attenuated response at the highest frequencies. Even with generation crystals as thick as 500 μm and a using a detection crystal of 300 μm, we observe frequencies extending up to 7.5 THz, although the presence of minima in the frequency domain is now very obvious. These are caused by phase mismatching in the generation crystal. THz radiation originating from different parts of the generation crystal may not necessarily add up constructively because the phase velocity of THz radiation and group velocity of the pump pulse are not equal. This temporal walk off becomes more dominant as the crystal thickness increases and can cause complete cancellation at some frequencies [19]. The reason for the cut-off seen around 7.5-8 THz is not related to phase matching. Rather, this is caused by the finite laser pulse duration of 50 fs, as we will show below. In practice, the use of crystals of 300 μm or thicker, is clearly an advantage compared to the use of the more fragile 100 μm crystals. The slow quasi-oscillatory background visible in Fig. 2(c) and Fig. 3(c) is caused by a slight movement of the pump beam by the loud speaker. Some of the ”modulated” pump light reaches the detector and gives rise to a background signal which is synchronous with the loudspeaker. After calibration and fourier transformation this slow oscillation will appear as low frequency content in the THz spectrum as seen on Fig’s 2 and 3 below 40 GHz.

We emphasize that the results are obtained without using any lock-in technique and without flushing the set-up with dry nitrogen gas. Notably absent in our measurement is the ringing

#98668 - $15.00 USD Received 11 Jul 2008; revised 4 Aug 2008; accepted 5 Aug 2008; published 7 Aug 2008

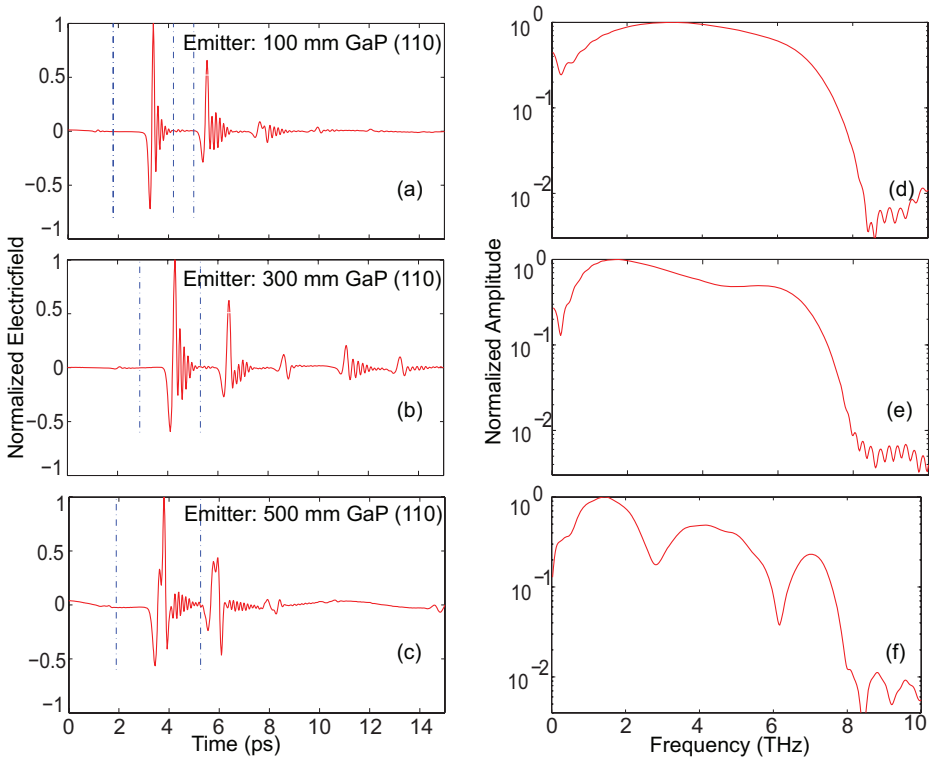

Fig. 3. Measured temporal wave forms of THz pulses generated by a GaP (110) crystal and detected very close to the generation crystal with a 100 μm thick GaP (110) crystal (a)-(c)and their corresponding spectra (d)-(f). The figures are normalized to their maximum.

in the time domain caused by the absorption and re-mission of the THz radiation by water vapor molecules. The optical path length of 1 mm between the two crystals is too small to observe any significant water vapor absorption. The closeness of the two crystals might wrongly suggest that the detection crystal is almost in the near-field region of the emitter. However, for the frequencies shown in Fig.'s 2 and 3 this distance is several wavelengths, and thus clearly beyond the near-field. The term quasi-near field is therefore more appropriate. If we define the signal to noise ratio (SNR) as the ratio of peak to peak THz electric field to the root mean square (rms) value of the noise when THz beam is blocked, we achieved a SNR of ≈ 450 in a total measurement time of less than a minute. We have compared our measurements with a conventional THz generation and detection set-up using a generation and a detection crystal, tens of centimeters apart, with a standard set of four parabolic mirrors in between. After a difficult alignment and optimization procedure, we then obtained a maximum SNR only half as large as with the quasi near-field method. In addition this set-up required vigorous flushing with dry N_2 gas to reduce THz absorption by water vapor molecules.

Another important point to note is that the probe and THz pulses are initially counter propagating and, after reflection, co-propagating in the detection crystal. The detected signal should therefore consist of a counter- and a co-propagating part. However, in our calculation of THz spectra, shown below, we have assumed that the THz and probe pulses co-propagate in the

#98668 - $15.00 USD Received 11 Jul 2008; revised 4 Aug 2008; accepted 5 Aug 2008; published 7 Aug 2008

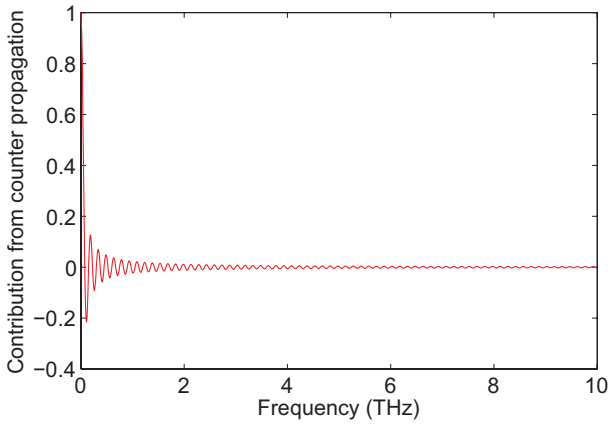

Fig. 4. The contribution to the measured electro-optic signal when the THz pulse and the probe pulse in the detection crystal are counter propagating as a function of THz frequency.

detection crystal. The agreement between the experiment and calculation strongly suggests that the effect of the counter propagating case to the electro-optic signal is negligible. Some insight can be gained by considering a very simple model in which we assume a delta function $\delta(z+v_g t)$ for the temporal intensity profile I_p of the probe pulse and a plane wave $E(z,t)=\cos(\omega t-k_T z)$ for the THz electric field. k_T is the THz wave vector along the z axis. The electro-optic signal measured is given by the following integral [20],

$$\Delta I \propto \int_0^{l_d} dz \int_{-\infty}^{\infty} dt I_p E(z,t) \tag{1}$$

If we assume, for the sake of argument, that the magnitudes of THz phase velocity and group velocity of the probe pulse are equal inside the detection crystal and, that the time delay between the THz pulse and probe pulse is zero, then,

$$\Delta I \propto \frac{E_0 l_d}{v_g}\left[\frac{\sin(2k_T l)}{2k_T l}\right] \tag{2}$$

In Fig. 4 we plot this contribution to the EO signal, normalized against the contribution of the co-propagating case, as a function of frequency for a 300 μm thick GaP crystal. The figure shows that the contribution from the counter propagating case is negligible at higher frequencies and shows increasingly larger amplitude oscillations versus frequency when the frequency decreases. Only for frequencies below a few hundred GHz the contribution to the signal increases to values larger than 10% . This should, perhaps, not come as a surprise. Electro-optic detection is a second-order non-linear optical process and when the two waves are counter propagating, this represents the largest possible phase mismatch and thus suggests an extremely low conversion process for all frequencies except the lowest.

#98668 - $15.00 USD Received 11 Jul 2008; revised 4 Aug 2008; accepted 5 Aug 2008; published 7 Aug 2008

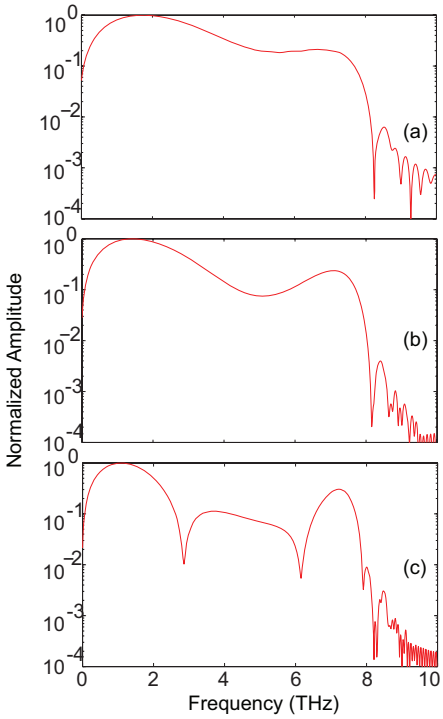

Fig. 5. Calculated spectra of THz radiation generated by GaP (110) crystal of thickness (a) 100 μm (b) 300 μm and (c) 500 μm and detected with 300 μm thick GaP (110) crystal. The calculation take phase matching effects and absorption of THz radiation in both generation and detection crystals into account.

To understand the origin of the shape and width of the THz amplitude spectrum, we have adapted a recently published model for THz pulse generation and detection [21]. The model includes: (i) the phase matching effect in both generation and detection crystal, (ii) absorption and dispersion of THz radiation in the generation crystal and detection crystal, (iii) Fabry-Perot reflections at the crystal surfaces, (iv) transmission of THz radiation at the crystal-air and air-crystal interfaces. Since our pump and probe pulse are $\approx$ 50 fs long, the dispersion of generating pulse in the generation crystal is negligible. The generated THz radiation is given by the expression

$$\begin{aligned} E_{Tg}(\omega) &= \frac{\sqrt{2}\pi\chi^{(2)}(\omega)}{n_T(\omega)^2-n_g^2}\tau_p E_0^2 exp\left[-\frac{\omega^2\tau_p^2}{4}\right]\left[\frac{1}{2}\left(1+\frac{n_g}{n_T(\omega)}\right)exp(i\omega n_T(\omega)l_g/c)\right. \\ &\left.+\frac{1}{2}\left(1-\frac{n_g}{n_T(\omega)}\right)exp(-i\omega n_T(\omega)l_g/c)-exp(i\omega n_g l_g/c)\right] \end{aligned} \quad (3)$$

where l_g is the thickness of the generation crystal, E_0 is the electric field amplitude of the pump pulse, ω is the THz radial frequency, n_g is the group refractive index of the pump pulse, τ_p is the pump and probe pulse duration at 1/e in intensity, $\chi^{(2)}(\omega) \propto [\varepsilon(\omega)-1]$, is the second order nonlinear susceptibility and $n_T(\omega)=\sqrt{\varepsilon(\omega)}$ is the complex refractive index of the material in the THz region. The dielectric function of the crystal in the THz frequency domain $\varepsilon(\omega)$ is given by [20]

#98668 - $15.00 USD Received 11 Jul 2008; revised 4 Aug 2008; accepted 5 Aug 2008; published 7 Aug 2008

$$\varepsilon(\omega) = \varepsilon_{el} + \frac{\varepsilon_{st}\omega_{TO}^2}{\omega_{TO}^2 - \omega^2 + 2i\gamma\omega} \tag{4}$$

where ε_{st} is the static dielectric constant, ω_{TO} is the angular frequency of TO phonon resonance, and γ is the damping factor. For GaP crystal $\omega_{TO} = 11$ THz, $\varepsilon_{st} = 2.03$, $\varepsilon_{el} = 9.09$ and $\gamma = 0.129$ THz. Eq. 3 takes into account the phase matching, absorption and dispersion of THz radiation in the generation crystal. The Fabry-Perot reflections at the crystal-air, air-crystal interfaces, coupling of THz radiation out of the generation crystal and coupling into the detection crystal can be described by the transfer functions. The reflection and transmission coefficients for the THz electric field at the crystal-air interface are:

$$\begin{aligned} R_{in}(\omega) &= (\sqrt{\varepsilon(\omega)} - 1)/(\sqrt{\varepsilon(\omega)} + 1) \\ T_{in}(\omega) &= 2/(\sqrt{\varepsilon(\omega)} + 1) \end{aligned}$$

At the air-crystal interface the coefficients are:

$$\begin{aligned} R_{out}(\omega) &= (1 - \sqrt{\varepsilon(\omega)})/(1 + \sqrt{\varepsilon(\omega)}) \\ T_{out}(\omega) &= 2\sqrt{\varepsilon(\omega)}/\sqrt{\varepsilon(\omega)} + 1 \end{aligned}$$

The transfer function for the Fabry-Perot effect in the generation and detection crystals are:

$$\begin{aligned} T_{fpg} &= 1/\left[1 + R_{out}^2 exp(i2n_T(\omega)\omega l_g/c)\right] \\ T_{fpd} &= 1/\left[1 + R_{in}^2 exp(i2n_T(\omega)\omega l_g/c)\right] \end{aligned}$$

The transfer function for the electro-optic sampling in the detection crystal is,

$$T_{eos} \propto \frac{c}{i\omega(n_T(\omega) - n_g)} \left[exp(il_d(n_T - n_g)\omega/c) - 1\right] exp\left(-\tau_p^2\omega^2/4\right) \tag{5}$$

The detected THz electric field is then given by

$$E_T(\omega) \propto E_{Tg} T_{out} T_{fpg} T_{in} T_{fpd} T_{eos} \tag{6}$$

Figure 5 shows the calculated spectra based on the above model. In the calculations we used 100 μm, 300 μm, 500 μm GaP (110) crystals for the generation and a 300 μm GaP (110) for detection. Overall, the calculated spectra show very good agreement with the experimental results shown in Fig. 2. Differences are observed at higher frequencies where the predicted amplitudes are higher than actually measured. A plausible explanation for this is that, in our calculation we do not take into account the group velocity dispersion of the laser pulses in both generation and detection crystals. However, a simulation shows that after propagation through a 300 μm GaP crystal, a 50 fs Gaussian pulse will be broadened to 60 fs. This explains why higher frequencies are less efficiently generated/detected in the experiment compared to the calculations.

The dips in the spectrum for the thickest emitter crystal can now be identified as phase matching minima. Our calculations also show that the bandwidth of the measured THz spectrum is completely determined by the pulse duration of the laser pulse. With the pulses emitted by our laser, frequencies higher than about 7.5 THz cannot be generated. Note that this bandwidth could be increased by using shorter pulses. However, shorter pulses will increasingly suffer from group velocity dispersion. This can lengthen the pulse considerably, and is, as stated before, not included in the model.

#98668 - $15.00 USD Received 11 Jul 2008; revised 4 Aug 2008; accepted 5 Aug 2008; published 7 Aug 2008

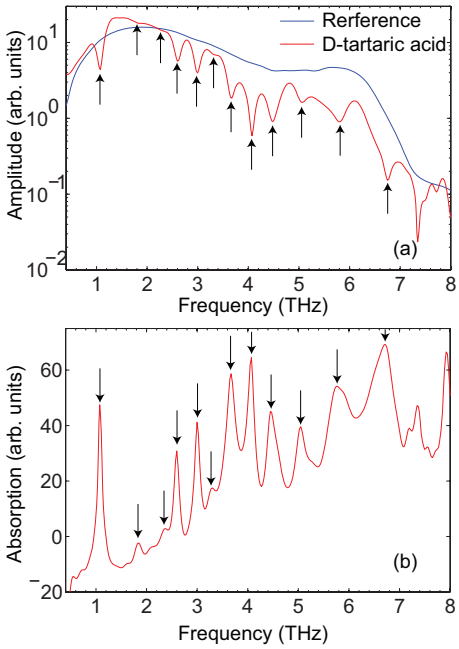

Fig. 6. (a) The frequency spectra measured with and without the D-tartaric acid pellet in between the generation and detection crystals. (b) The absorption spectrum of D-tartaric acid calculated from (a). The arrows indicate the THz absorption band positions.

Our setup is ideally suited to perform spectroscopy in the difficult to access frequency range of 0.5 to 7.5 THz. As an example we measured the absorption spectra of D-tartaric acid crystals. To prepare the sample, D-tartaric acid crystals are first ground using a mortar and pestle to reduce the particle size, so that light scattering is reduced to a minimum in the frequency range of interest. Polyethylene powder of particle size $\leq 30\ \mu$m (Mipelon XM-220, Mitsui Chemicals America, Inc) is mixed with the ground sample such that the the sample forms 30% of the total mass of the mixture. This is done to dilute the sample so that the absorption peaks are within the dynamic range of our system. The mixture is pressed into a pellet with a hydraulic press (Specac Ltd, UK). The pellets have a thicknesses of ≈ 0.6 mm.

In order to calculate the absorption spectrum of the sample, we measured THz electric fields with and without the sample in between the generation and detection crysals. To see the influence of the polyethylene powder on the absorption spectrum of D-tartaric acid, the absorption spectrum of a pure polyethylene pellet is also measured. It is found that polyethylene shows negligible absorption in our frequency range of interest. The absorption spectrum of D-tartaric acid measured with our set-up is shown in Fig. 6(b). It can be seen that the measured bandwidth extends up-to 7 THz. Our results are in agreement with earlier published spectra which measured the absorption of D-tartaric acid upto 3.5 THz [22, 23]. In Fig. 6(a), the electric field amplitude observed with the sample is higher than without the sample below 2.2 THz. This translates into an apparant negative absorption in Fig. 6(b). This is due to the fact that the lower frequencies suffer less diffraction when transmitted through the sample than through air, and are thus more effectively detected by the probe pulse. This problem can be reduced by using pump beams having a larger diameter or by decreasing the distance between the two crystals to a fraction of a wavelength, which will also increase the signal amplitude. This will reduce the

#98668 - $15.00 USD Received 11 Jul 2008; revised 4 Aug 2008; accepted 5 Aug 2008; published 7 Aug 2008

effects of diffraction of especially the lower frequency components.

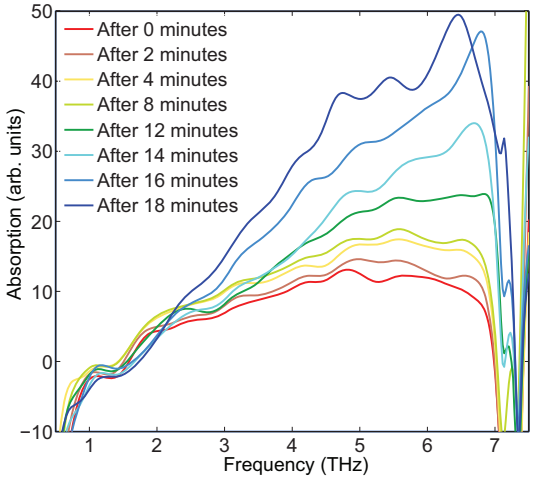

Fig. 7. The time evolution of the absorption spectrum of a freeze dried coffee sample at eight times after exposure to ambient air.

Access to frequencies >3 THz makes it easier to measure the increase or decrease in the water content of a hygroscopic material. As an example we show the absorption increase in the range from 0.5 - 7 THz of an initially freeze dried coffee sample, after being exposed to air. Freeze drying is a dehydration process. The frozen material is subjected to vacuum below the triple point of water. The thermal energy submitted to the material drives the sublimation process: the conversion from ice to water vapor without going through the liquid phase. This water vapor is subsequently removed by an ice condenser. When the crystalline water (ice) is removed, a highly porous structure is formed, which is very hygroscopic. The freeze dried coffee (IMA Edwards Freeze Drying Solutions) transforms from a dry spongy substance to a sticky substance in less than 20 minutes if exposed to ambient air. Figure 7 shows the absorption by the freeze dried coffee sample as a function of frequency, for several times after exposure to ambient air. Compared to the low frequency region, the frequency region between 3 - 7 THz gives a very clear indication of the increasing water content of the sample. In order to measure the water content quantitatively, the system should be calibrated with samples whose initial water content is known and stable, and the whole experiment should be conducted in a very controlled atmosphere, which is beyond the scope of this paper.

Finally, we would like to speculate on the application of pump beam modulation techniques to further improve the signal-to-noise ratio. As pointed out in the introduction, pump modulation techniques can create their own problems such as mechanical vibrations or pulse lengthening. If those problems can be minimized, then modulating the pump beam with consecutive lock-in detection, may lead to further improvements of the signal-to-noise ratio. An attempt by us to implement this using an elasto-optic modulator operating at a fixed frequency of 50 kHz failed, however, due to excessive pump laser noise in this modulation frequency range. It is likely that the future use of better modulation techniques will improve our current setup even further.

#98668 - $15.00 USD Received 11 Jul 2008; revised 4 Aug 2008; accepted 5 Aug 2008; published 7 Aug 2008

4. Conclusion

We have presented a simple and efficient way to generate and detect THz radiation with a large bandwidth of 7.5 THz without using lock-in techniques. In addition there is no need to flush the set-up with dry nitrogen gas because our set-up does not suffer from water vapor absorption. The observed spectra of the generated THz pulses are explained with a simple model which takes into account the effects of phase-matching and absorption of THz radiation in the generation and detection crystals. We have also shown that the effect of counter propagation of THz pulse and probe pulse in the detection crystal is negligible at higher frequencies. Samples as thick as a few millimeters can be inserted between the generator and detector crystals to perform spectroscopy. As an example we show the measured absorption spectrum of D-tartaric acid from 0.5 - 7 THz. We illustrate, with the example of a freeze dried coffee, that the changes in the moisture content are efficiently monitored at high THz frequencies.

Acknowledgments

This work was performed as part of the research program of the " Stichting voor Fundamenteel Onderzoek der Materie (FOM)," which is financially supported by the "Nederlandse Organisatie voor Wetenschappelijk Onderzoek (NWO). Research support from the EU TERANOVA Program (RCN-71835) is also acknowledged.

#98668 - $15.00 USD Received 11 Jul 2008; revised 4 Aug 2008; accepted 5 Aug 2008; published 7 Aug 2008